Epilepsy Research (2014) 108, 872—882

journal homepage: www.elsevier.com/locate/epilepsyres

Tractography of Meyer's Loop asymmetries

Patricia Dreessen de Gervai[a], Uta N. Sboto-Frankenstein[b,*], R. Bruce. Bolster[a,c], Sunny Thind[a], Marco L.H. Gruwel[d], Stephen D. Smith[a,c], Boguslaw Tomanek[b,e]

[a] *National Research Council Institute for Biodiagnostics, Magnetic Resonance Technology, 435 Ellice Avenue, Winnipeg, MB R3B 1Y6, Canada*
[b] *Alberta Innovates Technology Futures, 435 Ellice Avenue, Winnipeg, MB R3B 1Y6, Canada*
[c] *Biopsychology Program, Department of Psychology, University of Winnipeg, 515 Portage Avenue, Winnipeg, MB R3B 2E9, Canada*
[d] *National Research Council Aquatic and Crop Resource Development, 435 Ellice Avenue, Winnipeg, MB R3B 1Y6, Canada*
[e] *Multimodal and Functional Imaging Group, Central Europe Institute of Technology, Kamenice 753, Brno CZ-62500, Czech Republic*

Received 17 June 2013; received in revised form 24 January 2014; accepted 16 March 2014
Available online 26 March 2014

KEYWORDS
Meyer's Loop;
Asymmetry;
Optic radiations;
Diffusion tensor imaging

Summary
Purpose: The purpose of the current study was to use diffusion tensor imaging (DTI) to conduct tractography of the optic radiations (OR) and its component bundles and to assess both the degree of hemispheric asymmetry and the inter-subject variability of Meyer's Loop (ML). We hypothesized that there are significant left versus right differences in the anterior extent of ML to the temporal pole (TP) in healthy subjects.
Materials and methods: DTI data were acquired on a 3 T Siemens MRI system using a single-shot Spin Echo EPI sequence. The dorsal, central and ML bundles of the OR were tracked and visualized in forty hemispheres of twenty healthy volunteers. The uncinate fasciculus (UF) was also tracked in these subjects so that it could be used as a distinct anatomical reference. Measurements were derived for the distance between ML-TP, ML and the temporal horn (ML-TH) and ML and the uncinate fasciculus (ML-UF). Paired difference *t*-tests were carried out with SPSS 14.0.
Results: ML and the UF were successfully tracked and visualized in all 20 volunteers. Significant hemispheric asymmetries were found for all measurements with left distances shorter than the right ($P < 0.005$). In 50% of the subjects the left ML-UF distance was $\leq$1.9 mm.

* Corresponding author. Tel.: +1 204 230 2629.
E-mail address: UtaFrankenstein@sboto.com (U.N. Sboto-Frankenstein).

http://dx.doi.org/10.1016/j.eplepsyres.2014.03.006

Conclusion: The results support our hypothesis and demonstrate that left ML-TP distances are significantly shorter than right ML-TP distances. These asymmetries are also reflected in shorter left distances between ML-TH and ML-UF. Moreover, these results are of interest to left-sided temporal lobe epilepsy surgery because it is not only more likely to disturb the anterior extent of ML but also renders the often closely located posterior aspect of the left UF more vulnerable to potential surgical impact

Introduction

One of the most common complications of temporal lobe epilepsy (TLE) surgery is a partial or complete superior homonymous quadrantanopia (Chen et al., 2009; Jeelani et al., 2010; Jensen and Seedorf, 1976; Marino and Rasmussen, 1968; Taoka et al., 2008; Van Buren and Baldwin, 1958; Yeni et al., 2008; Yogarajah et al., 2009). This defect is due to the disruption of the anterior bundle of the optic radiation (OR) commonly known as Meyer's Loop (ML) (Meyer, 1907).

ML is part of the OR (also known as the geniculocalcarine tract) and is the ventral bundle of axons originating from neurons in the lateral geniculate nucleus (LGN) of the thalamus. Together with the central and dorsal bundles of the OR, ML passes through the retrolenticular portion of the internal capsule to bring visual input to the occipital cortex on both sides of the calcarine sulcus (Carpenter, 1991). Two of the three fibre bundles use the shortest route to reach the occipital cortex. The central bundle moves laterally from the LGN and projects posteriorly along the external wall of the lateral ventricle to project central vision to the occipital cortex both above and below the calcarine fissure. Similarly, the dorsal bundle takes the shortest route via a direct posterior projection of the lower visual field to the upper area of the calcarine cortex. By contrast, ML curves forward first, loops towards the tip of the temporal horn (TH) and turns sharply to project posteriorly to carry visual input from the upper field to the region below the calcarine fissure. It is this particular temporal-anterior trajectory that demonstrates notable anatomical variability across individuals and thus poses challenges for TLE surgery and the minimization of neurological deficit (Chen et al., 2009; Ebeling and Reulen, 1988; Jeelani et al., 2010; Taoka et al., 2008; Yeni et al., 2008; Yogarajah et al., 2009).

Diffusion tensor imaging (DTI) is the only imaging tool that allows the noninvasive and in vivo visualization of white matter (WM) fibre tracts such as the OR and its component bundles. In structured tissues, such as central nervous system WM, there is a preferred direction of water diffusion (diffusion is anisotropic) that enables the analysis of diffusion properties of water molecules within nerve fibres (Basser and Pierpaoli, 1996). In structured tissues, such as central nervous system WM, there is a preferred direction of water diffusion imposed by barriers such as axonal membranes and myelin sheaths. DTI is an MRI technique based on diffusion weighted imaging. Combining diffusion weighted images, obtained in many different directions, allows the calculation of the water diffusion tensor in each voxel. High anisotropy of the tensor values indicates geometric restrictions for water movement, permitting estimation of the location and trajectory of fibre tracts. Deterministic tractography performed on these data sets connects nearest neighbours with similar anisotropy values to form streamlines.

Although there are a number of dissection studies (Burgel et al., 1999; Ebeling and Reulen, 1988; Kier et al., 2004; Rubino, 2005; Sincoff et al., 2004) and tractography (Chen et al., 2009; Choi et al., 2006; Nilsson et al., 2007, 2010; Sherbondy et al., 2008; Taoka et al., 2008; Yamamoto et al., 2005, 2007; Yogarajah et al., 2009; Wang et al., 2011; Winston et al., 2011) that have explored the anatomy of ML, there is considerable variability in reports of the exact location, trajectory, volume and hemispheric asymmetry of the tract. For example, in dissection studies the distance of the most anterior extent of ML to the temporal pole (ML-TP) is usually shorter compared to tractography studies. Tractography studies of the ML demonstrate variability in distance measurements depending on the type of analysis used (Nilsson et al., 2010; Winston et al., 2011) as well as trends towards a shorter ML-TP distance in the left hemisphere (Yogarajah et al., 2009). This is in agreement with a study of neurosurgical cases conducted by Jeelani et al. (2010) who reported left greater than right ML asymmetries and visual field deficits (VFD) that are 3.5 times more likely following left-sided surgery. Another neurosurgical study showed that left-sided surgery resulted in VFD in 6 out of 11 patients compared to 3 out of 10 with right-sided surgery (Yogarajah et al., 2009). The potential for significant hemispheric asymmetry of ML has also been recently suggested in a thorough review on the challenges of the anatomy and tractography of ML (Mandelstam, 2012).

Few DTI studies, generally with small-study cohorts, have assessed ML-TP hemispheric asymmetries in healthy control subjects (Nilsson et al., 2007; White and Zhang, 2010; Wu et al., 2012). The largest study with healthy subjects was conducted by Yogarajah et al. (2009) who used probabilistic analysis methods. These authors reported a trend towards a shorter left ML-TP distance across patient and control groups. The aim of the current study was to assess both the degree of hemispheric asymmetry and the inter-subject variability of ML. Specifically we hypothesized that there would be significant left versus right differences in the anterior extent of ML towards the TP. To further delineate the potential asymmetry of ML across hemispheres we also report asymmetry measurements between ML and the TH as well as the most posterior aspect of the uncinate fasciculus (ML-UF). The original contribution of our work is the demonstration of significant asymmetries of ML, not only in relation to the TP, but also to the TH and UF.

Methods

Subjects

Our study enrolled twenty neurologically healthy volunteers (10 males and 10 females, mean age 22.5 ± 2.66 (range 19—30)), all with self-reports of right-handedness from the University of Winnipeg. The study was approved by the ethics committees of the National Research Council of Canada and the University of Winnipeg and informed written consent was obtained from all subjects. All participants completed MR safety screening prior to entry to the magnet. All work was carried out in accordance with The Code of Ethics of the World Medical Association (Declaration of Helsinki).

MR data acquisition

MRI studies were performed on a 3 T Siemens TIM-TRIO MRI scanner at the National Research Council Institute for Biodiagnostics (NRC IBD) MR facility in Winnipeg. For both anatomical and DTI a 12-channel phased array head matrix coil was used. To prescribe the DTI a whole brain volumetric T1-weighted (MP-RAGE) spoiled gradient-echo sequence was used: 1 slab with 176 slices and a 0.5 mm gap, slice thickness: 1 mm, in plane resolution: 1.0 mm × 1.0 mm, TR/TE: 1900/2.2 ms, flip angle: 9^{O}, acquisition matrix: 256 × 256, FOV: 240 mm × 240 mm.

The DTI sequence was a single-shot Spin Echo (SE) EPI sequence provided by Siemens. The scanning parameters were as follows: imaging plane: axial, phase encoding direction: A-P; echo spacing: 0.82 ms, TE: 93 ms, TR: 9100 ms; number of slices: 66, inter-slice gap: 0 mm; bandwidth: 1396 Hz/pixel, voxel size: 1.9 mm × 1.9 mm × 1.9 mm; acquisition matrix: 128 × 128, NEX: 4. Images were acquired with *b* values of 0 and 1000 s/mm^2 in 20 directions following an icosahedral scheme. Parallel acquisition using GRAPPA (generalized autocalibrating partially parallel acquisition) with an effective acceleration factor of 2 was used for an acquisition time of 13 min 13 s.

Data analysis

The first step was the preprocessing and analysis of diffusion data with the conversion of DICOM images into a 4D Nifti file and corresponding bvecs and bvals. For this step we used Chris Rorden's dcm2nii converter in MRICron (Rorden et al., 2007). Eddy Current correction was performed using the FDT module of the FSL Software Library (FMRIB Centre, University of Oxford, Oxford, United Kingdom) (Smith et al., 2004). These eddy current and motion-corrected files were used for tractography in MedINRIA (Medical Image Navigation and Research Tool by INRIA, 06902 Sophia Antipolis CEDEX, France; http://www.sop.inria.fr.asclepios/software/-MedINRIA) (Fillard et al., 2007).

Region of interest placement for tractography

Initially, individual tractography was performed separately for the right and left OR, as a whole structure, in each subject (OR-entire tract). In a second step, three additional inclusive target Regions of Interest (ROIs) were placed to separate ML and the central and dorsal bundles (OR-separate bundles). ROIs were selected based on the correspondence between anatomical knowledge of the separate bundles (Ebeling and Reulen, 1988) and their visualization using the ConTrack DTI-FT algorithm (Sherbondy et al., 2008).

OR-entire tract

To track the OR as a whole, coronal and axial views of the directionally encoded fractional anisotropy (DEC-FA) maps were used to identify the LGN (caudal and lateral to the pulvinar nucleus of the thalamus). To ensure that the entire OR was circumscribed, the first ROIs were placed in the axial plane extending over five consecutive slices (Fig. 1a displays the central slice, ROI 1, which was placed at the level of the anterior commissure, see small arrow). This ensured inclusion of all fibres (predominantly red in the DEC-FA map) arising from the LGN projecting laterally (Fig. 1c). Three exclusion ROIs were placed to exclude fibres that did not belong to the OR. The first exclusion ROI was placed mid-sagittally to exclude fibres crossing from the splenium of the corpus callosum. The second exclusion ROI was placed in the axial plane at the level of the pons to avoid the inclusion of fibres from the corticospinal tract. A third exclusion ROI was placed in the coronal view at the anterior limit of the temporal horn to eliminate fibres from neighbouring bundles which include the fronto-occipital, the uncinate and inferior longitudinal fasciculi as well as the anterior commissure.

OR-separate bundles

To track the three separate bundles of the OR, the LGN ROI (ROI 1) as described above was used as the first inclusion (Fig. 1a). The second inclusion ROIs (ROI 2, 3 and 4) were prescribed in the coronal plane and were segregated along the dorsal-ventral axis based on the anatomical projection of the individual bundles along the sagittal stratum as described below.

For ML the second inclusive ROI (ROI 2, Fig. 1b) was placed in the coronal view in the inferior sagittal stratum (parallel to the posterior horn of the lateral ventricle). This intersected all the horizontal fibres that belong to ML. These run anteriorly towards the tip of the inferior horn, pass posteriorly along the lateral wall of the ventricle and end on the lower lip of the calcarine fissure (Fig. 1f). For the identification of the central bundle (ROI 3, Fig. 1b), the second inclusive ROI was also placed in the sagittal stratum, at midlevel. The central bundle has mostly oblique fibres that leave the LGN in a lateral direction. It takes a posterior direction along the lateral wall of the ventricle, and from there radiates towards the visual cortex (Fig. 1e). For the dorsal bundle the second inclusive ROI (ROI 4, Fig. 1b) was placed in the superior area of the sagittal stratum. The dorsal bundle follows a straight direction to meet the upper area of the primary visual cortex (Fig. 1d).

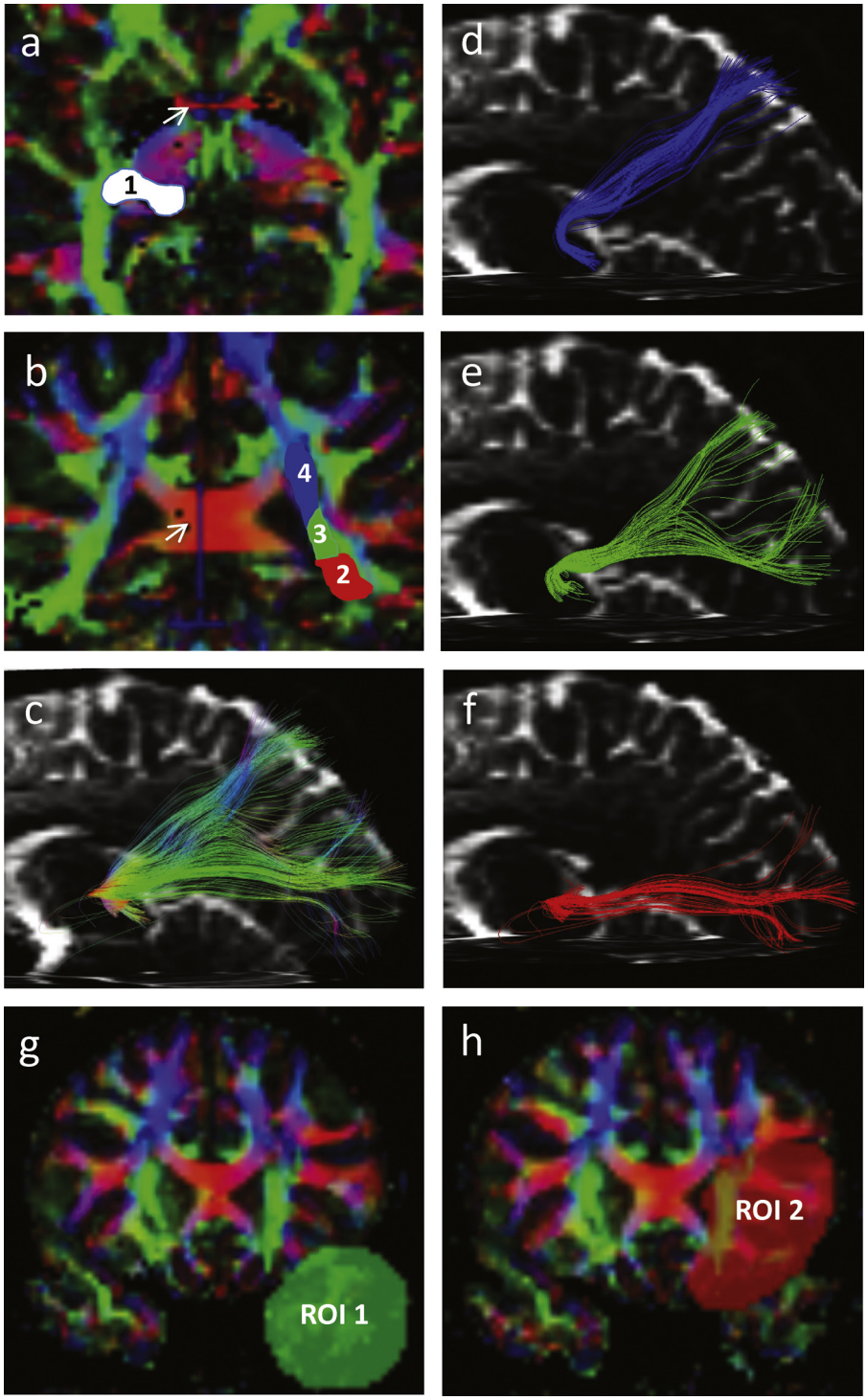

Figure 1 Inclusion ROIS for the OR, ventral, central and dorsal bundles and the uncinate fasciculus. (a) Depicts the central slice of the LGN volume ROI (1) used to track the entire OR in (c). The LGN volume ROI (1) was drawn in 5 slices in the axial plane with the middle slice at the level of the anterior commissure (see arrow in a). ROI 1 in combination with ROIS 2, 3 or 4 (drawn in the coronal plane at the level of the splenium of the corpus callosum, see arrow in b) and the visual assessment of the entire OR in (c) were used to track the dorsal, central and ventral bundles (d—f). (g) and (h) show the coronal planes used to draw the temporal (ROI 1) and frontal (ROI 2) inclusion ROIs for the UF tractography. All ROIs are drawn on directionally encoded FA maps and tracts are depicted superimposed on the $b = 0\,s/mm^2$ image. (For interpretation of the references to colour in the text, the reader is referred to the web version of the article.)

Uncinate fasciculus
For the UF the first inclusive ROI was placed in the coronal plane around the temporal lobe at the level of the genu of the corpus callosum (GCC). For some subjects this ROI was placed slightly posterior to the GCC to capture the temporal lobe. A second inclusive coronal ROI was placed one slice posterior to the first inclusion ROI still at the level of the GCC in the frontal lobe. These ROIs are depicted in Fig. 1g—h. Additional exclusionary ROIs were used to isolate UF fibres. The first exclusion ROI was drawn in the sagittal plane over the midline to avoid fibres crossing from the contralateral hemisphere. A second exclusion ROI was drawn in the coronal plane right behind the most posterior aspect of the UF to avoid inclusion of fibres from the inferior longitudinal fasciculus.

Asymmetry measurements

For all subjects and both hemispheres distances were measured between the anterior extent of ML and: 1. the most posterior aspect of the UF as it curves upward to the orbitofrontal cortex (ML-UF), 2. the anterior terminus of the temporal horn (ML-TH) and 3. the TP, (ML-TP). The TH and TP landmarks were identified on the $b = 0\,s/mm^2$ image. The UF was tracked and also loaded onto the $b = 0\,s/mm^2$ image for distance measurements between ML-UF. Fig. 2 provides a depiction of the distance measurements in three representative subjects. Paired difference *t*-tests were carried out with SPSS 14.0 to compare distance measurements between the left and right hemispheres. We also assessed the effect of sex on distance measurement asymmetries. Results were reported as significant if they had a *P* value ≤ 0.05.

Results

Using the methods described above we were able to successfully track the OR with its three separate component bundles consisting of ML, the central and dorsal bundles in twenty healthy volunteers. ML was successfully tracked in all subjects and there were pronounced individual differences in the symmetry of the temporal-anterior extent of the tract. The UF was also successfully tracked in all subjects, distances between ML, the UF, TH and TP were measured in 40 temporal lobes and significant differences were observed between hemispheres. There were no significant differences in male/female measurements.

Asymmetry measurements

Table 1 reports the individual and grouped asymmetry measurements between ML-UF, ML-TH and ML-TP in both hemispheres. Distance measurements were conducted in forty temporal lobes.

ML-TP distances of individual subjects were rank ordered with the most symmetric ML-TP distance (0 mm) observed in subject 1 (see Table 1 and Fig. 3) and the most asymmetric ML-TP distance (16.9 mm) observed in Subject 20 (see Table 1 and Figs. 3 and 4).

Significant hemispheric differences were found for all three comparisons ($P \leq 0.00273$).

Overall, ML-TP distances were significantly different between the left and right hemisphere measurements ($P \leq 0.00273$). Left ML-TP distances were shorter compared to right ML-TP distances.

ML-TH distances were significantly different between the left and right hemisphere measurements ($P \leq 0.00038$), with left ML-TH distances shorter than the right.

ML-UF distances were significantly different between the left and right hemisphere measurements ($P \leq 0.00038$). On the left side ML and UF overlapped in one subject (S18). By contrast the right side in the same subject showed an ML-UF distance of 16.9 mm. Left ML-UF distances $\leq$1.9 mm were observed in 10 subjects (S4,7, S13—20), with right-sided distances typically measuring $\geq$11.3 mm (an exception was S7 who had an ML-UF distance of 3.8 mm). In S10 these results were reversed with overlapping ML-UF tracts on the right side (−1.9 mm) and an ML-UF distance of 11.3 mm on the left side. For all subjects there were no significant asymmetries between the UF-TP distances.

A representation of these distance asymmetries can be observed in Fig. 2 where both the ML and UF tracts are overlaid onto the $b = 0\,s/mm^2$ image. Fig. 2 displays three representative subjects. Fig. 2a and b shows S19 with a clear leftward ML-UF asymmetry. The yellow arrow in Fig. 2b points towards the minimal distance (1.1 mm) between ML and the UF in the left hemisphere, and the yellow line depicts the distance (18.8 mm) between the anterior extent of ML and the posterior extent of the UF in the right hemisphere. Fig. 2c shows S7 with more symmetric ML-UF distances. The yellow arrows point towards the distances between the right and left ML and the UF. Finally Fig. 2d shows S10 which is our only subject with a clear rightward asymmetry of ML-UF. The right ML-UF distance is shorter (−1.9 mm, delineated by the yellow arrow) than the left ML-UF distance (11.3 mm, delineated by the yellow line).

Distance measurements

Averaged across hemispheres, the mean distance between ML-TP was 42.9 mm (range 28.1—54.4 mm). The mean distance of ML-TH is 13.7 mm (range 3.8—24.4 mm) and the mean distance of ML-UF was 10.5 mm (range 3.8—20.6 mm).

Tractography

Subjects were grouped into two figures for display purposes only. Combining all 20 subjects into one figure reduces the size of the individual images so that it becomes too difficult to visually assess the degree of asymmetry.

Figs. 3 and 4 show that the tractography is consistent with the known anatomical course of the OR in general and ML in particular. In all subjects the ML originates from the LGN and projects anteriorly across the superior aspect of the anterior tip of the lateral ventricle's temporal horn. ML then curves sharply in the posterior direction and joins the medial and dorsal bundles that run along the wall of the lateral ventricle and terminate in the lower, medial and dorsal aspects of the calcarine cortex. The dorsal (blue), medial (green) and ML (red) bundles follow the expected trajectory of the OR. Individual differences can be observed in the proportions of the component bundles of the OR and all but one subject

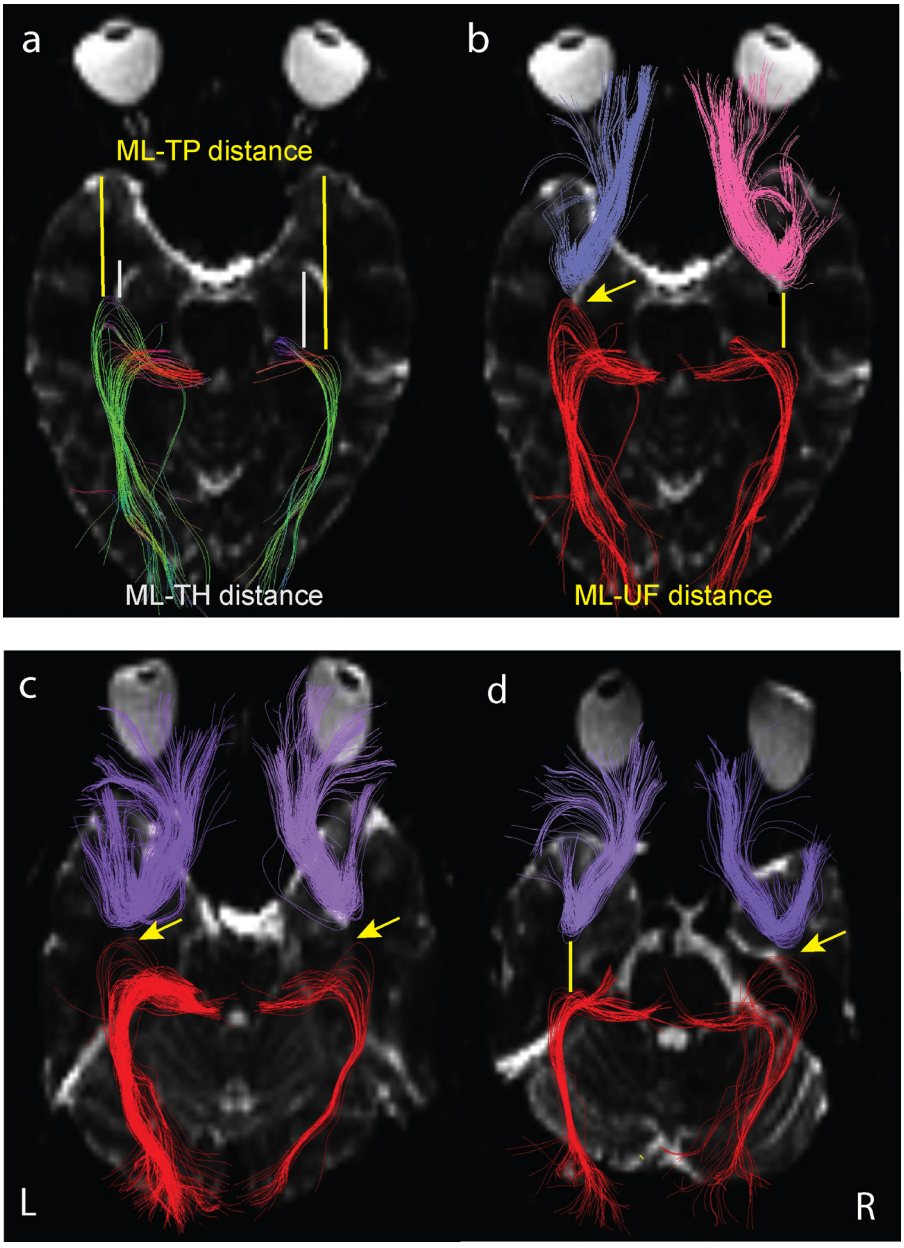

Figure 2 ML distance measurements (a—d) and examples of ML-UF tractography (b—d). ML-TP distances (yellow lines) and ML-TH distances (grey lines) are displayed on a $b = 0\,s/mm^2$ image with the corresponding directionally encoded ML (a). ML-UF distances with a leftward asymmetry (see yellow arrow) are depicted in (b). Symmetrical ML-UF distances (yellow arrows in c) and rightward asymmetrical ML-UF distances (yellow arrow in d). (For interpretation of the references to colour in this figure legend, the reader is referred to the web version of the article.)

demonstrate degrees of asymmetry in the temporal-anterior extent of ML.

Fig. 3 shows the tractography of the three bundles of the OR in nine subjects with ML-TP asymmetry measurements ranging from 0 to 6.2 mm. Fig. 4 shows the tractography of the OR in eleven subjects with ML-TP asymmetry measurements $\geq$7.5 mm. While subjects 11—20 demonstrate leftward asymmetry of ML, subject 10 is the only subject where rightward asymmetry can be clearly visualized. In subjects 10—14, 15, 19 and 20 the anterior extent of ML is clearly visible. The remaining four subjects show relatively sparse ML streamlines.

Discussion

There is general consensus on the individual variability of the exact location, anatomy, course and hemispheric symmetry of ML (Chen et al., 2009; Ebeling and Reulen, 1988; Mandelstam, 2012). Keeping in mind that deterministic tractography has been criticized to overestimate ML-TP distances, the present study is the first to report significant asymmetries in the anterior extent of ML. These significant asymmetries are supported by significant differences in three distinct inter-hemispheric distance measurements: ML-TP, ML-TH and ML-UF.

Table 1

		Distances (mm)								
	Subject	ML-TP			ML-UF			ML-TH		
Symmetry		right	left	right-left	right	left	right-left	right	left	right-left
	1	45	45	***0***	13.2	11.3	1.9	16.9	9.4	7.5
	2	42.6	43	***-0.4***	13.1	13.1	0	15	15	0
	3	46.9	45	***1.9***	20.6	15.2	5.4	16.9	15	1.9
	4	37.5	35.6	***1.9***	11.3	0	11.3	13.1	18.5	-5.4
	5	46.9	48.8	***-1.9***	16.9	13.1	3.8	24.4	20.6	3.8
	6	46.9	48.8	***-1.9***	18.8	13.1	5.7	18.8	18.8	0
	7	38.1	35.9	***2.2***	3.8	1.9	1.9	9.4	3.7	5.7
	8	54.4	48.8	***5.6***	16.9	16.9	0	18.8	16.9	1.9
	9	36.9	43.1	***-6.2***	16.9	15	1.9	18.8	15	3.8
	10	28.1	35.6	***-7.5***	-1.9	11.3	-13.2	3.8	11.3	-7.5
	11	48.8	41.3	***7.5***	16.9	11.3	5.6	24.4	15	9.4
	12	52.5	45	***7.5***	18.8	5.6	13.2	18.8	7.5	11.3
	13	39.4	30	***9.4***	11.3	1.9	9.4	9.4	3.8	5.6
	14	46.9	35.6	***11.3***	13.1	1.8	11.3	18.8	5.6	13.2
	15	48.8	37.5	***11.3***	13.1	1.9	11.2	22.5	5.6	16.9
	16	46.9	34.2	***12.7***	15	1.9	13.1	20.6	5.6	15
	17	46.9	33.8	***13.1***	15	1.9	13.1	22.5	5.6	16.9
	18	52.5	37.5	***15***	16.9	-3.8	20.7	16.9	5.6	11.3
	19	50.6	33.8	***16.8***	18.8	1.1	17.7	15	3.8	11.2
Asymmetry	20	52.5	35.6	***16.9***	15	0	15	20.6	3.8	16.8
Mean		**45.46**	**39.70**	**5.76**	**14.18**	**6.73**	**7.45**	**17.27**	**10.31**	**6.97**
SD		**6.60**	**5.82**	**7.48**	**5.29**	**6.50**	**7.73**	**5.25**	**5.93**	**7.23**
P-Value			**0.00273**			**0.000379**			**0.000379**	

Asymmetry measurements

ML-TP distance

Asymmetry measurements in the current study support our hypothesis and demonstrate that the mean ML-TP distance is significantly shorter in the left (39.70 mm) compared to the right (45.64 mm) temporal lobe (Table 1). The asymmetry of the anterior extent of the OR has been initially discussed in dissection studies (Ebeling and Reulen, 1988), and representative figures of the OR in dissection and tractography studies often depict leftward asymmetry (Govindan et al., 2008; Hofer et al., 2010; Mandelstam, 2012; Sherbondy et al., 2008). Consistent with the significant leftward asymmetry of ML-TP in our study, Burgel et al. (1999) report significant leftward asymmetries of the LGN and OR in a dissection study of ten adult human brains. To date there have only been a few DTI studies that have assessed ML-TP asymmetries in healthy control subjects (Nilsson et al., 2007; Yogarajah et al., 2009; Wu et al., 2012). While some DTI studies with smaller cohorts do not establish asymmetries of ML (Nilsson et al., 2007; Wu et al., 2012), the largest study by Yogarajah et al. (2009) reports a trend towards the left ML-TP distance being smaller than the right across patient and control groups. The authors further demonstrated that both the size of the anterior temporal lobe resection and the anterior extent of the OR are predictors of the occurrence and severity of postoperative visual field deficits. This is in agreement with a neurosurgical study conducted by Jeelani et al. (2010) who report left greater than right ML asymmetries and visual field deficits that are 3.5 times more likely following left-sided surgery. Taken together, these studies support our findings of significant leftward asymmetries of ML.

In a recent review Mandelstam (2012) suggests that there may be significant hemispheric asymmetries within individuals and cites studies that have postulated that a leftward asymmetry of the OR may be due to expanded language areas in the left posterior temporal lobe that have displaced the OR on that side (Jeelani et al., 2010; Wang et al., 2008). 95% of right-handed individuals have left lateralized language function. Although handedness was not formally assessed in our study, all subjects gave self-reports of right-handedness. If expanded language areas in the left posterior temporal lobe have displaced the OR and pushed ML forward we would expect the majority of right-handed subjects to show leftward ML asymmetries. Keeping in mind that handedness was not formally assessed in our study all but six of our self-reported right-handed subjects showed a leftward ML asymmetry. Of these six subjects one showed no asymmetry (S1), three showed asymmetries $\leq$1.9 mm (S2, 5 and

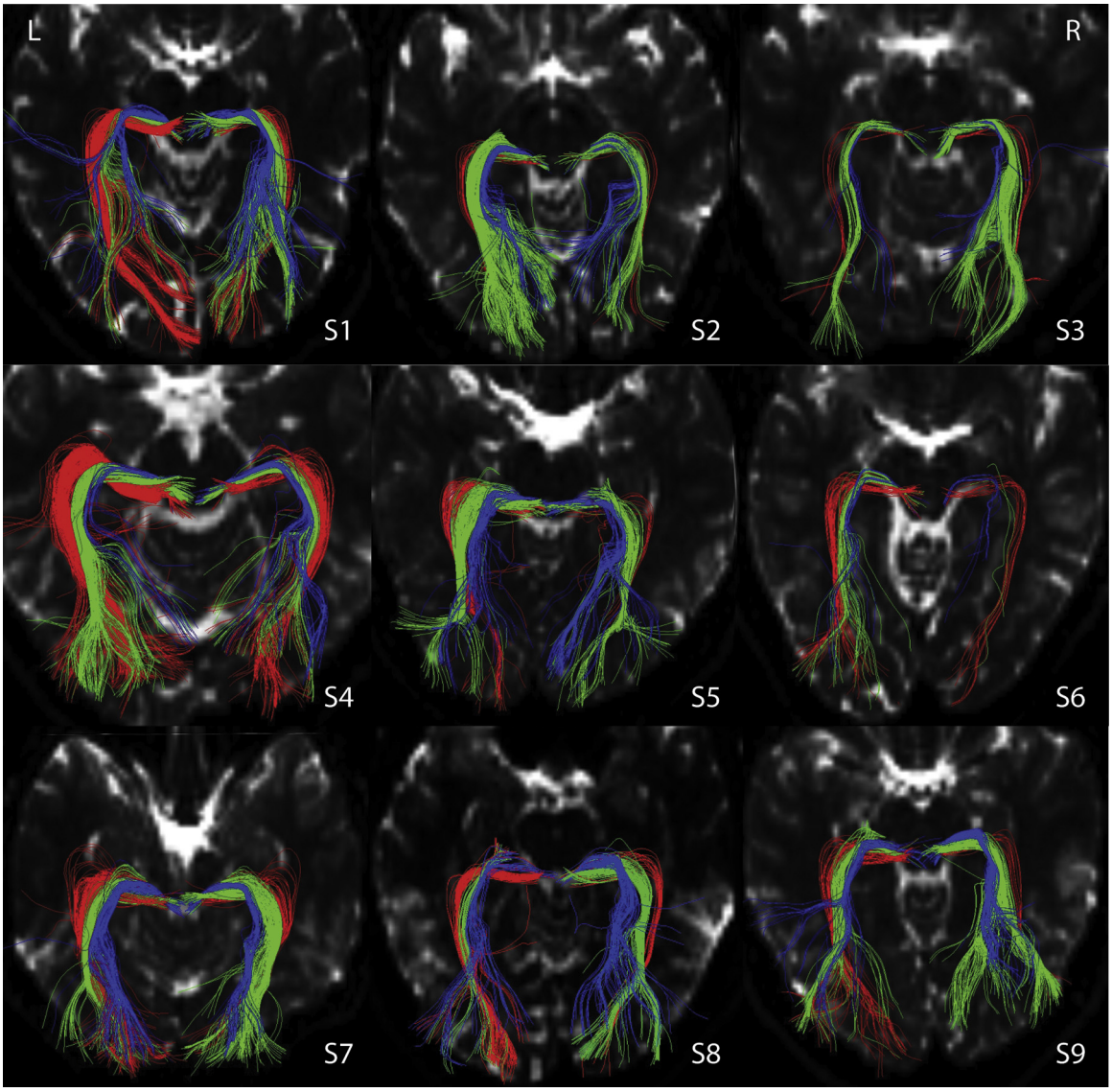

Figure 3 Tractography of the three component bundles of the OR in 9 subjects with ML asymmetries $\leq$6.2 mm. ML is seen in red, the central bundle in green and the dorsal bundle in blue. All tracts are overlaid onto the $b = 0\,s/mm^2$ image. (For interpretation of the references to colour in this figure legend, the reader is referred to the web version of the article.)

6) while the remaining two showed rightward asymmetry (S9 and S10) (see Table 1).

ML-UF distance

Further support for the demonstrated ML-TP asymmetries in the current study comes from the significant hemispheric differences in ML-UF distances (Table 1). Taoka et al. (2008) used tractography of the UF and proposed that the UF is located ''just anterior'' to the most anterior tip of ML and can thus be used to better delineate its most anterior point. Fifty percent of his patients did not demonstrate a gap between the posterior limit of the UF and the anterior limit of ML and none of the patients showed an ML-UF distance greater than 4 mm. Consistent with their findings, our results show that the most posterior aspect of the UF was located within or below 2 mm of the most anterior aspect of ML in 11 subjects. Out of these, 2 subjects had a 0 mm distance between ML-UF, and 2 subjects demonstrated an overlap between ML-UF. Contrary to the results reported by Taoka et al. (2008) our group observed significant differences between the left and right ML-UF distance measurements, with shorter gaps between the left ML-UF (mean = 6.73 mm) and longer gaps between the right ML-UF (mean = 14.18 mm) tracts. Fig. 2 provides examples of left (Fig. 2a and b) and rightward (Fig. 2d) ML-UF asymmetry and more symmetric ML-UF distances (Fig. 2c), in three representative subjects. Our results place the anterior aspect of ML in the left hemisphere closer to the posterior aspect of the UF, suggesting that DTI tracking of the UF may provide a more reliable and conservative marker for the anterior extent of ML in the left hemisphere than either TP or TH. These results also suggest that left-sided TLE surgery poses a larger risk for neurological deficit, not only involving ML but potentially also the UF. This is further supported by a DTI TLE

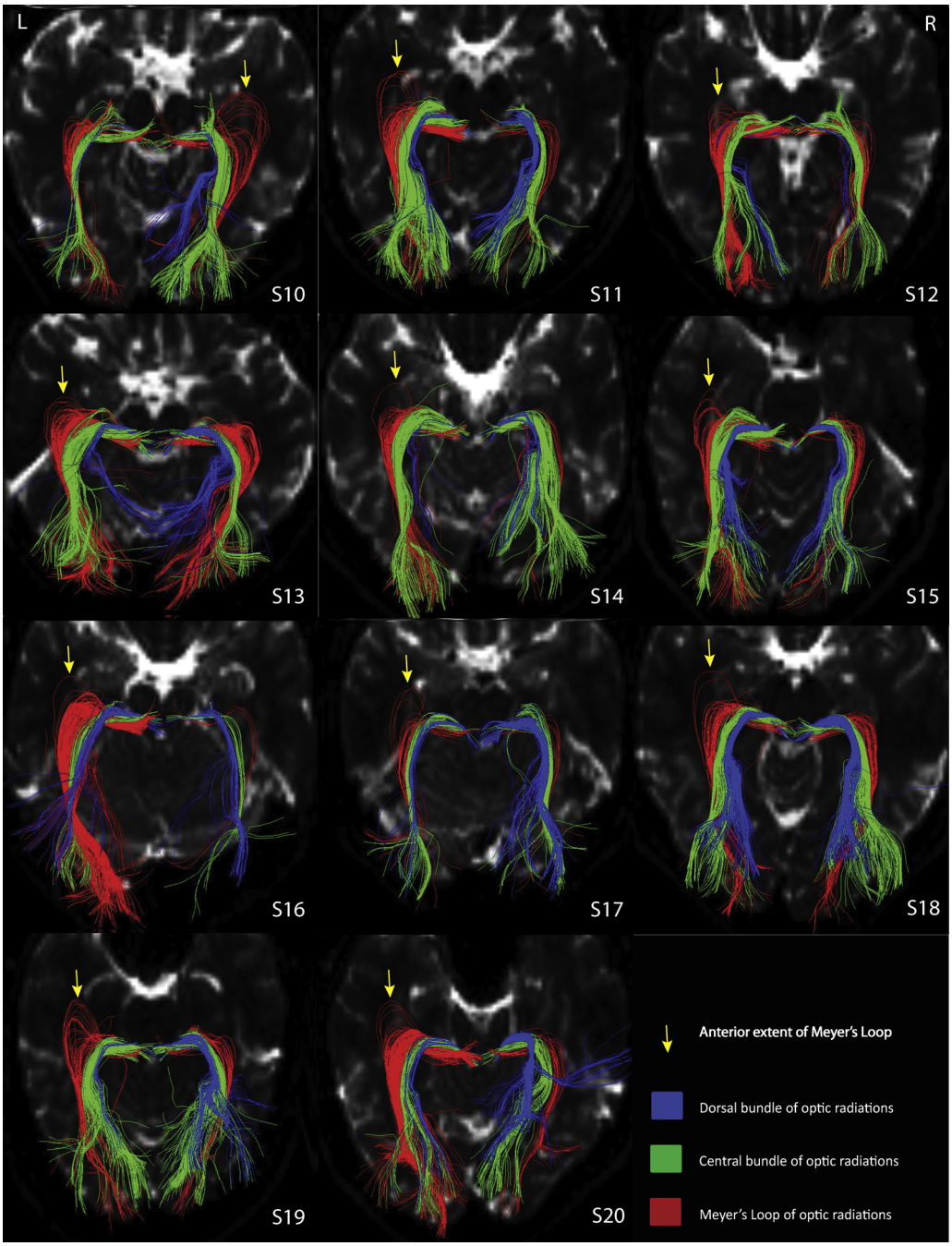

Figure 4 Tractography of the three component bundles of the OR in 11 subjects with ML asymmetries $\geq$7.5 mm (see yellow arrows). ML is seen in red, the central bundle in green and the dorsal bundle in blue. All tracts are overlaid onto the $b = 0\,s/mm^2$ image. (For interpretation of the references to colour in this figure legend, the reader is referred to the web version of the article.)

study by Diehl et al. (2008) who report that damage to the left UF, based on diffusion parameter measurements, is associated with reduced performance on measures of auditory immediate and delayed memory in left TLE patients.

Distance measurements

Exact knowledge of the ML-TP distance is necessary to minimize its overestimation and thus decrease the potential for post-operative VFDs. The overall distance between ML-TP in this study is 42.9 mm, which is comparable to measurements reported by Nilsson et al. (2007, 2010) (44 mm, 41 mm) and Wu et al. (2012) (40.2 mm) using deterministic tractography. However, these measurements are high in contrast to other deterministic tractography studies that report ML-TP distances that are $\leq$37.3 mm (Chen et al., 2009; Taoka et al., 2008; Yamamoto et al., 2005; Yogarajah et al., 2009; for review see Mandelstam, 2012). Indeed, streamline algorithms have been criticized due to their

high false negative rate (Mandelstam, 2012; Sherbondy et al., 2008). Probabilistic tractography algorithms allow for multiple pathways for each DTI sample point and direct comparisons of deterministic and probabilistic tractography report longer ML-TP distances using the former (mean 41 mm, range 34—51 mm) versus the latter (mean 30 mm, 17—42 mm) technique (Nilsson et al., 2010). Others have reported ML-TP mean distances of 28 mm (Sherbondy et al., 2008) 30 mm (Nilsson et al., 2010) and 35 mm (Yogarajah et al., 2009) using probabilistic tractography. Probabilistic measures therefore more closely approximate values ($\leq$31.4 mm) obtained with gold standard dissection techniques (Choi et al., 2006; Ebeling and Reulen, 1988; Pujari et al., 2008; Rubino, 2005). Probabilistic tractography is less likely to underestimate the anterior extent of ML because it assigns a probability function to multiple local pathway orientations, increasing the ability to track fibre trajectories with a high degree of curvature. The anterior portion of ML has a tightly looping trajectory, which means fibres may fall below thresholds for angular resolution of streamline tracking in deterministic methods. Nevertheless, the use of deterministic tractography in the current study is the only one to date demonstrating significant hemispheric asymmetries in ML-TP, TH and UF distances. Therefore we propose that probabilistic methods result in shorter ML-TP distances, however, both, deterministic and probabilistic tractography will demonstrate significant laterality differences.

Limitations

The main limitation of this study is that the measurements reported were derived from deterministic tractography and may therefore overestimate the ML-TP distance. Together with Nilsson et al. (2007) and Wu et al. (2012) our mean distance of the most anterior position of ML is at least 1 cm posterior to estimates from dissection studies (Ebeling and Reulen, 1988). This concern attaches to the absolute distance for any particular measure when comparing deterministic tractography to dissection studies, and thus our measures should not be adopted as hard guidelines for surgical intervention. Nevertheless this should have no bearing on the relative distances when comparisons are made across hemispheres when using deterministic tractography. We were able to track the OR and its three component bundles and provide evidence that supports our hypothesis of significant hemispheric asymmetries of ML.

Chen et al. (2009) demonstrated that there was considerable shifting of the OR during surgery, without a common pattern of brain shift. Therefore tractography in healthy volunteers and even presurgical tractography in TLE patients may lead to erroneous assumptions about the exact location of ML. Intra-operative tractography may provide further insight into the exact location of ML after the skull has been opened and therefore decrease the incidence of postoperative VFDs in TLE patients with ATL surgery. However, fast and accurate tracking algorithms will be needed to provide tractography that can be useful within a clinical time frame.

Apart from tractography analysis methods, there are MR acquisition factors that can greatly impact the signal to noise ratio (SNR) and thus contribute to the visualization of ML in this study. Magnetic field strength, the sequence used, the strength of the gradients and the number of gradient directions, the type of coil, the voxel size and the use of parallel imaging all contribute to the results obtained in this study and have been thoroughly reviewed by others (Alexander et al., 2006; Mukherjee et al., 2008). We obtained small isotropic voxels, used four averages to optimize the SNR, applied parallel imaging (GRAPPA) to minimize distortions associated with EPI sequences and applied 20 gradient directions to visualize the OR and in particular the anterior extent of ML in our study.

Conclusion

In conclusion, we have demonstrated that deterministic tractography is an effective tool to document significant hemispheric asymmetries of the anterior extent of ML in a group of twenty healthy volunteers. This asymmetry was further supported by the anatomical relationship of ML with the TP, TH and the UF. The ML-UF distance measurements validated the ML asymmetries in that right ML-UF distances were significantly longer than left ML-UF distances. Furthermore the posterior aspect of the left UF was in very close proximity (<1.9 mm) to the anterior extent of ML in 50% of our subjects, suggesting that left-sided TLE can benefit from the presurgical visualization of both ML and the UF.

Acknowledgments

The research was supported by grants from the Manitoba Health Research Council Establishment Grant and a Natural Sciences and Engineering Research Council of Canada Discovery Grant to Stephen Smith.

References

Alexander, A.L., Lee, J.E., Wu, Y.-C., Field, A.S., 2006. Comparison of diffusion tensor imaging measurements at 3.0 T versus 1.5 T with and without parallel imaging. Neuroimaging Clin. N. Am. 16 (2), 299—309.

Basser, P.J., Pierpaoli, C., 1996. Microstructural and physiological features of tissues elucidated by quantitative-diffusion-tensor MRI. J. Magn. Reson. Ser. B 111 (3), 209—219.

Burgel, U., Schormann, T., Schleicher, A., Zilles, K., 1999. Mapping of histologically identified long fibre tracts in human cerebral hemispheres to the MRI volume of a reference brain: position and spatial variability of the optic radiation. Neuroimage 10, 489—499.

Carpenter, M., 1991. Core Text of Neuroanatomy, 4th ed. Williams & Wilkins, Baltimore, MD (Chapter 9).

Chen, X., Weigel, D., Ganslandt, O., Buchfelder, M., Nimsky, C., 2009. Prediction of visual field deficits by diffusion tensor imaging in temporal lobe epilepsy surgery. Neuroimage 45 (2), 286—297.

Choi, C., Rubino, P.A., Fernandez-Miranda, J.C., Abe, H., Rhoton Jr., A.L., 2006. Meyer's loop and the optic radiations in the transsylvian approach to the mediobasal temporal lobe. Neurosurgery 59 (4 Suppl. 2), ONS228—ONS235, discussion ONS235—ONS236.

Diehl, B., Busch, R.M., Duncan, J.S., Piao, Z., Tkach, J., Luders, H.O., 2008. Abnormalities in diffusion tensor imaging of the uncinate fasciculus relate to reduced memory in temporal lobe epilepsy. Epilepsia 49 (8), 1409—1418.

Ebeling, U., Reulen, H.-J., 1988. Neurosurgical topography of the optic radiation in the temporal lobe. Acta Neurochir. (Wien) 92, 29—36.

Fillard, P., Penne, X., Arsigny, V., Ayache, N., 2007. Clinical DT-MRI estimation, smoothing and fibre tracking with log-Euclidian metrics. IEEE Trans. Med. Imaging 26 (11), 1472—1482.

Govindan, R.M., Chugani, H.T., Makki, M.I., Behen, M.E., Dornbush, J., Sood, S., 2008. Diffusion tensor imaging of brain plasticity after occipital lobectomy. Pediatr. Neurol. 38 (1), 27—33.

Hofer, S., Karaus, A., Frahm, J., 2010. Reconstruction and dissection of the entire human visual pathway using diffusion tensor MRI. Front. Neuroanat. 4 (15), 1—7.

Jeelani, N.u.O., Jindahra, P., Tamber, M.S., Poon, T.L., Kabasele, P., James-Galton, M., Stevens, J., Duncan, J., McEvoy, A.W., Harkness, W., Plant, G.T., 2010. 'Hemispherical asymmetry in the Meyer's Loop': a prospective study of visual-field deficits in 105 cases undergoing anterior temporal lobe resection for epilepsy. J. Neurol. Neurosurg. Psychiatry 81 (9), 985—991.

Jensen, I., Seedorf, H., 1976. Temporal lobe epilepsy and neuro-opthalmology. Opthalmological findings in 74 temporal lobe resected patients. Acta Opthal 54, 827—840.

Kier, E.L., Staib, L.H., Davis, L.M., Bronen, R., 2004. MR imaging of the temporal stem: Anatomic Dissection tractography of the uncinate fasciculus, inferior occipitofrontal fasciculus, and Meyer's Loop of the optic radiation. Am. J. Neuroradiol. 25, 677—691.

Nilsson, D., Starck, G., Ljungberg, M., Ribbelin, S., Jonsson, L., Malmgren, K., Rydenhag, B., 2007. Intersubject variability in the anterior extent of the optic radiation assessed by tractography. Epilepsy Res. 77, 11—16.

Nilsson, D., Rydenhag, B., Malmgren, K., Starck, G., Ljundberg, M., 2010. Anatomical accuracy and feasibility of probabilistic and deterministic tractography of the optic radiation. Epilepsia 51 (Suppl. 4), 91.

Mandelstam, S.A., 2012. Challenges of the anatomy and diffusion tensor tractography of the Meyer Loop. Am. J. Neuroradiol. 33 (7), 1204—1210.

Marino, R., Rasmussen, T., 1968. Visual field changes after temporal lobectomy in man. Neurology 18, 825L 835.

Meyer, A., 1907. The connections of the occipital lobes and the present status of the cerebral visual affections. Trans. Assoc. Am. Physicians 22, 7—16.

Mukherjee, P., Chung, S.W., Berman, J.I., Hess, C.P., Henry, R.G., 2008. Diffusion tensor MR imaging and fibre tractography: technical considerations. Am. J. Neuroradiol. 29 (5), 843—852, http://dx.doi.org/10.3174/ajnr.A1052.

Pujari, V.B., Jimbo, H., Dange, N., Shah, A., Singh, S., Goel, A., 2008. Fibre dissection of the visual pathways: analysis of the relationship of optic radiations to lateral ventricle: a cadaveric study. Neurol. India 56 (2), 133—137.

Rubino, A.L.R., 2005. Three-dimensional relationships of the optic radiation. Neurosurgery 57 (4 Suppl.), 219L 27.

Rorden, C., Karnath, H.-O., Bonilha, L., 2007. Improving Lesion-Symptom Mapping. J. Cogn. Neurosci. 19 (7), 1081—1088.

Sherbondy, A.J., Dougherty, R.F., Napel, S., Wandell, B.A., 2008. Identifying the human optic radiation using diffusion imaging and fibre tractography. J. Vision 8 (10).

Sincoff, E.H., Tan, Y., Abdulrauf, S.I., 2004. White matter fibre dissection of the optic radiations of the temporal lobe and implications for surgical approaches to the temporal horn. J. Neurosurg. 101 (5), 739—746.

Smith, S.M., Jenkinson, M., Woolrich, M.W., Beckmann, C.F., Behrens, T.E.J., Johansen-Berg, H., Bannister, P.R., De Luca, M., Drobnjak, I., Flitney, D.E., Niazy, R.K., Saunders, J., Vickers, J., Zhang, Y., De Stefano, N., Brady, J.M., Matthews, P.M., 2004. Advances in functional and structural MR image analysis and implementation as FSL. Neuroimage 23 (Suppl. 1), S208—S219.

Taoka, T., Sakamoto, M., Nakagawa, H., Nakase, H., Iwasaki, S., Takayama, K., Taoka, K., Hoshida, T., Sakaki, T., Kichikawa, K., 2008. Diffusion tensor tractography of the Meyer Loop in cases of temporal lobe resection for temporal lobe epilepsy: correlation between postsurgical visual field defect and anterior limit of Meyer Loop on tractography. Am. J. Neuroradiol. 29 (7), 1329—1334.

Van Buren, J.M., Baldwin, M., 1958. The architecture of the optic radiation in the temporal lobe of man. Brain 81 (1), 15—40.

Wang, F., Sun, T., Li, X., Xia, H., Li, Z., 2011. Microsurgical and tractographic anatomical study of insular and transsylvian transinsular approach. Neurol. Sci. 32 (5), 865—874.

Wang, F., Sun, T., Li, X.-G., Liu, N.-J., 2008. Diffusion tensor tractography of the temporal stem on the inferior limiting sulcus: laboratory investigation. J. Neurosurg. 108 (4), 775—781.

White, M.L., Zhang, Y., 2010. Three-Tesla diffusion tensor imaging of Meyer's loop by tractography, color-coded fractional anisotropy maps, and eigenvectors. Clin. Imaging 34 (6), 413—417.

Winston, G.P., Mancini, L., Stretton, J., Ashmore, J., Symms, M.R., Duncan, J.S., Yousry, T.A., 2011. Diffusion tensor imaging tractography of the optic radiation for epilepsy surgical planning: a comparison of two methods. Epilepsy Res. 97 (1—2), 124—132.

Wu, W., Rigolo, L., O'Donnell, L.J., Norton, I., Shriver, S., Golby, A., 2012. Visual pathway study using in vivo diffusion tensor imaging tractography to complement classic anatomy. Oper. Neurosurg. 70, 145—156.

Yamamoto, A., Miki, Y., Urayama, S., Fushimi, Y., Okada, T., Hanakawa, T., Fukuyama, H., Togashi, K., 2007. Diffusion tensor fiber tractography of the optic radiation: analysis with 6-, 12-, 40-, and 81 directional motion-probing gradients, a preliminary study. Am. J. Neuroradiol. 28, 92—96.

Yamamoto, T., Yamada, K., Nishimura, T., Kinoshita, S., 2005. Tractography to depict three layers of visual filed trajectories to the calcarine gyri. Am. J. Ophthalmol. 140, 781—785.

Yeni, S.N., Tanriover, N., Uyanik, Ö., Ulu, M.O., Özkara, Ç., Karaağaç, N., Ozyurt, E., Uzan, M., 2008. Visual field defects in selective amygdalohippocampectomy for hippocampal sclerosis. Neurosurgery 63 (3), 507—515.

Yogarajah, M., Focke, N.K., Bonelli, S., Cercignani, M., Acheson, J., Parker, G.J.M., Duncan, J.S., 2009. Defining Meyer's loop-temporal lobe resections, visual field deficits and diffusion tensor tractography. Brain: J. Neurol. 132 (Pt 6), 1656—1668.